Yuzuncu Yil University Journal of the Institute of Natural & Applied Sciences

https://dergipark.org.tr/en/pub/yyufbed

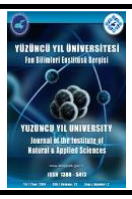

Research Article

Hierarchical $MnSb_2O_6$ Particles for Dispersive Solid-Phase Extraction of Co(II) from Wastewater by Flame Atomic Absorption Spectrometry

Dilges BASKIN*

Van Yüzüncü Yıl University, Muradiye Vocational School, Chemistry and Chemical Processing Technologies Department, 65080, Van, Turkey

*Corresponding author e-mail: dilgesbskn@gmail.com

Abstract: The efficacy of hierarchical $MnSb_2O_6$ magnetic flower-shaped particles (MFSP) as adsorbents for the determination of metal ions using flame atomic absorption spectrometry (FAAS) was evaluated through dispersive solid-phase extraction (DSPE) in this study. Key parameters, including pH, sorbent amount, mixing type and duration, eluent type and volume, and sorbent type (magnetic and non-magnetic) were optimized to improve DSPE–FAAS performance. The MFSP–DSPE–FAAS method demonstrated a dynamic linear range of 5.0–100 ng mL^{-1} for Co^{2+} ions with a correlation coefficient of 0.9996. Moreover, the magnetic sorbent–DSPE–FAAS method exhibited an 86-fold increase in sensitivity for Co^{2+} compared to FAAS alone, underscoring the significant contribution of the hierarchical magnetic flower-shaped particles in achieving selective and efficient adsorption. A recovery study using a wastewater (domestic effluent) sample from the General Directorate of VASKİ (Van Water and Sewerage Administration) yielded recoveries between 94% and 108%. This study highlights, for the first time, the combined use of magnetic $MnSb_2O_6$ and non-magnetic SbO_2 flower-shaped particles to reveal the role of magnetic properties in DSPE performance and to validate their applicability in real wastewater analysis. The developed method not only addressed the challenges posed by complex environmental matrices but also demonstrated the crucial role of magnetic properties in facilitating efficient metal ion adsorption.

Keywords: Cobalt determination, Dispersive solid-phase extraction, Environmental analysis, Flame atomic absorption spectrometry

Alevli Atomik Absorpsiyon Spektrometresi ile Atık Su Matrisinde Kobalt(II) Tayini için Hiyerarşik $MnSb_2O_6$ Parçacıklarının Dağılımlı Katı Faz Ekstraksiyonunda Kullanımı

Öz: Bu çalışmada, hiyerarşik yapılı $MnSb_2O_6$ manyetik çiçek-şekilli parçacıkların (MFSP) alevli atomik absorpsiyon spektrometresi (AAAS) ile metal iyonlarının tayininde adsorban olarak etkinliği, dağılımlı katı faz ekstraksiyonu (DKFE) yöntemi kapsamında değerlendirilmiştir. pH, adsorban miktarı, karıştırma türü ve süresi, elüent tipi ve hacmi ile adsorban türü (manyetik ve manyetik olmayan) gibi parametreler optimize edilerek DKFE–AAAS performansı iyileştirilmiştir. MFSP–DKFE–AAAS yöntemi, Co^{2+} iyonları için 5.0–100 ng mL^{-1} aralığında dinamik bir doğrusal çalışma aralığı sunmuş ve korelasyon katsayısı 0.9996 olarak elde edilmiştir. Ayrıca, manyetik adsorban kullanılan yöntem doğrudan AAAS'a kıyasla 86 kat daha yüksek duyarlılık göstermiştir. Van Su ve Kanalizasyon İdaresi'nden (VASKİ) temin edilen atık su (evsel atıksu) örneği ile yapılan geri kazanım çalışmasında %94–108 aralığında başarılı sonuçlar elde edilmiştir. Bu çalışma, ilk kez manyetik $MnSb_2O_6$ ve manyetik olmayan SbO_2 çiçek şeklindeki parçacıkların birlikte kullanımını, manyetik özelliklerin DSPE performansındaki rolünü ortaya koymak ve gerçek atıksu analizlerinde uygulanabilirliğini doğrulamak için rapor etmektedir. Geliştirilen yöntem, çevresel matrislerin analizinde karşılaşılan zorlukları aşmada etkili

Received Date: 13.06.2025
Accepted Date: 29.10.2025

How to cited: Baskın, D. (2025). Hierarchical $MnSb_2O_6$ particles for dispersive solid-phase extraction of Co(II) from wastewater by flame atomic absorption spectrometry. *Yuzuncu Yil University Journal of the Institute of Natural and Applied Sciences,, 30*(3), 907-921. https://doi.org/10.53433/yyufbed.1718800

olmuş ve manyetik özelliklerin metal iyonlarının seçici ve verimli adsorpsiyonundaki belirleyici rolünü ortaya koymuştur.

Anahtar Kelimeler: Alevli atomik absorpsiyon spektrometrisi, Çevresel analiz, Dağılımlı katı faz ekstraksiyonu, Kobalt tayini

1. Introduction

Heavy metals are an important group of pollutants that must be monitored due to their widespread occurrence in daily life and their adverse health effects (Rehman et al., 2018). They can be found in water, soil, food, and even cosmetic products (Baskın et al., 2021; Cimboláková et al., 2020), and may be highly toxic even at trace amounts (Ali et al., 2019). Continuous exposure to heavy metals such as Pb, Cd, Co, Cu, As, and Hg leads to bioaccumulation in the human body, which can result in serious health problems including developmental delays and cognitive impairments in children, kidney and liver damage in adults, and increased cancer risk (Ali et al., 2019; Bhargava et al., 2017; Wehmeier et al., 2024). Even modest exposure can have severe long-term consequences. Among these, cobalt is particularly noteworthy because of its extensive use in alloys, electroplating, and rechargeable batteries, which increases its likelihood of release into wastewater and necessitates sensitive monitoring strategies (Lin et al., 2021). For this reason, the development of reliable trace-level detection methods is crucial to ensure compliance with legal safety limits. However, the determination of heavy metals in real matrices is often complicated by matrix effects due to the presence of organic and inorganic interferents (Baskin, 2025a; Mafakheri et al., 2024).

Moreover, many heavy metals exist in environmental samples at ultra-trace levels, which requires preconcentration strategies before determination (Oviedo et al., 2024; Salamat & Soylak, 2024). Dispersive solid-phase extraction (DSPE) is one of the most widely applied methods for this purpose. DSPE employs a solid sorbent material to selectively adsorb the target analyte while minimizing the co-extraction of interferents (Baskin, 2025b; Hagarová & Nemček, 2021). The technique is advantageous due to its simplicity, selectivity, and high enrichment factors, making it particularly suitable for complex environmental samples (Sürme et al., 2024).

In recent years, nanosized and microstructured structures have garnered attention due to their large surface area and tunable surface functionalities (Alav et al., 2024). These properties enhance the adsorption and desorption kinetics of the nano-sized sorbents. Materials with flower-shaped or hierarchical morphologies are especially attractive due to their high density of active sites, providing faster and more efficient extraction compared to bulk sorbents (Ahmadi et al., 2017; Azzouz et al., 2018; Büyüktiryaki et al., 2020a, 2020b; Keçili & Hussain, 2018). By tailoring the surface chemistry, size, and morphology, customized sorbents can be developed to achieve selective and sensitive analyses in both environmental and biological monitoring.

Among various sorbent candidates, metal oxides with unique morphologies have been extensively studied because of their chemical stability, high adsorption capacity, and low cost (da Costa et al., 2024; Haghighi & Kazemi, 2021; Tong et al., 2019). Manganese oxides are attractive due to their high adsorption potential, magnetic properties, and environmental friendliness (Li et al., 2023; Öner et al., 2023).On the other hand, antimony oxides have gained attention because of their variable morphology and strong chemical stability (Qi et al., 2022). Recent studies have reported the successful application of MnO_2-based sorbents (Ali & Azzam, 2023) and Sb-oxide nanoparticles (İnce et al., 2024) in trace metal preconcentration and real sample matrices. The combination of manganese and antimony oxides into hierarchical $MnSb_2O_6$ offers the advantages of both systems, but their use as pristine sorbents in DSPE has been scarcely reported in the literature.

In this study, we developed a dispersive solid-phase extraction method using hierarchical $MnSb_2O_6$ flower-shaped particles (magnetic) and compared their performance with SbO_2 particles (non-magnetic) for the enrichment of Co^{2+} ions. This direct comparison has not been previously reported and represents the novelty of our approach. The primary aim was to investigate whether magnetic properties provide an additional benefit in selective adsorption. Both sorbents were synthesized and characterized using X-ray diffraction (XRD), high-resolution transmission electron microscopy (HRTEM), field emission scanning electron microscopy (FESEM), and energy-dispersive X-ray spectroscopy (EDX).

Furthermore, the effect of the sample matrix was assessed by applying the method to real wastewater samples.

2. Materials and Methods

The experimental studies were conducted using analytical grade reagents, including HNO_3, antimony trichloride ($SbCl_3$), and manganese(II) chloride ($MnCl_2$), which were procured from AB Chemical (Turkey). A standard stock solution of cobalt (1000 mg L^{-1}) was obtained from High-Purity Standards (Charleston, SC, USA) and diluted as required to prepare working solutions. Buffer solutions were prepared using potassium hydrogen phthalate (pH 3–6), tris (pH 7), borax (pH 8–10), and disodium hydrogen phosphate (pH 11–12), together with NaOH and HCl (Merck). Zeta potential of flower-shaped particles (MFSP) dispersions was determined by electrophoretic light scattering (ELS, Malvern Zetasizer Nano ZS). For each measurement, 20 mg of sorbent was dispersed in 50 mL ultrapure water by sonication for 5 min to obtain a stable suspension. The pH of the suspensions was adjusted to the desired values (7.0–10.0) using small volumes of 0.1 M NaOH or HCl. Measurements were performed at 25 °C, and each data point represents the average of three replicates.

Ultrapure water was supplied by a Merck Millipore Direct-Q 3 UV system and used for all dilutions. A flame atomic absorption spectrophotometer (Thermo Scientific ICE-3000 series, USA) was employed to quantify Co^{2+} ions. A cobalt hollow cathode lamp was used as the radiation source, with an operating current of 5.0 mA and a spectral bandpass of 0.5 nm. Measurements were carried out at the analytical wavelength of 240.7 nm. Acetylene was used as the fuel gas at a flow rate of 1.0 L min^{-1}, and air was used as the oxidant to generate a stoichiometric flame.

For characterization of the synthesized particles, X-ray diffraction (XRD) patterns of SbO_2 and $MnSb_2O_6$ were obtained on a Rigaku Ultima-IV diffractometer using Cu Kα radiation (λ = 1.5406 Å) at 30 kV, with a scan range of 2θ = 10–90°. High-resolution transmission electron microscopy (HRTEM, JEOL-JEM 2100) was employed for crystal and morphological characterization. Field emission scanning electron microscopy (FESEM, Zeiss Sigma VP 300) was used to observe the three-dimensional morphology, and an energy-dispersive X-ray (EDX, Ametek EDAX) detector coupled to the FESEM provided elemental mapping of $MnSb_2O_6$. $MnSb_2O_6$ particles (and SbO_2 where noted) were investigated by X-ray photoelectron spectroscopy (XPS, Thermo Scientific K-Alpha) operated at 12 kV.

2.1. Synthesis of hierarchical $MnSb_2O_6$ particles

The hierarchical $MnSb_2O_6$ particles were synthesized using a hydrothermal method adapted from (Tong et al., 2019). Briefly, 30 mL of an aqueous solution containing $MnCl_2$ and $SbCl_3$ (1:4 molar ratio) was prepared under magnetic stirring. The resulting solution was transferred into a Teflon-lined stainless steel autoclave and maintained at 180 °C for 3 h. The obtained yellow precipitate was centrifuged and washed five times with ultrapure water until a neutral pH (≈7) was reached. The product was then dried at 70 °C for 12 h, yielding hierarchical magnetic $MnSb_2O_6$ particles.

For comparison, non-magnetic SbO_2 particles were also synthesized following the same procedure. Thus, two types of sorbents ($MnSb_2O_6$ and SbO_2) were obtained to evaluate the role of magnetic properties in the preconcentration of Co^{2+} ions. This design allowed the analyte–adsorbent interaction to be interpreted in terms of both morphology and magnetism.

2.2. Extraction procedure

The preparation of standard solutions containing Co^{2+} ions for extraction and calibration experiments was carried out meticulously. A 1000 mg L^{-1} Co^{2+} stock solution was purchased and diluted to the desired concentrations for each experiment. The optimum sample volume (45 mL, either standard solution or real sample) was adjusted to the desired pH with an appropriate buffer solution. Flower-shaped particles were then introduced into the buffered analyte solution and mixed to enhance the interaction between the sorbent and analyte.

Following centrifugation at 6000 rpm, the particles were separated at the bottom of the centrifuge tube, and the supernatant was carefully decanted. To desorb the retained analyte, 300 µL of concentrated HNO_3 (optimized eluent) was added, followed by vortex mixing for 30 s. The resulting

solution was collected after centrifugation and analyzed by FAAS under optimized instrumental conditions.

For example, in the optimized MFSP–DSPE–FAAS procedure for Co^{2+}, a 50 ng mL^{-1} Co^{2+} solution was mixed with 1.5 mL of pH 10 buffer and 40 mg of MFSP sorbent. Manual shaking for 60 s was applied to increase contact between the analyte and sorbent. After centrifugation and decantation, 300 µL of HNO_3 was added to the sorbent, vortexed for 30 s, and then centrifuged again at 6000 rpm. The eluent was collected for FAAS measurement.

The optimal values of the studied parameters, including pH, sorbent type and quantity, eluent type and volume, and mixing type and duration, are summarized in Table 1. The method was validated in terms of limit of detection (LOD), limit of quantification (LOQ), coefficient of determination (R^2), and relative standard deviation (%RSD).

The slope (S) of the calibration line was determined within the linear range. The standard deviation (SD) was calculated from seven replicate measurements at the lowest concentration tested. The LOD and LOQ were then calculated using the following equations:

$$LOD = 3.3 \times {}^{SD}/_{S} \quad (1)$$

$$LOQ = 10 \times {}^{SD}/_{S} \quad (2)$$

The validation results confirmed that the method exhibited satisfactory performance.

2.3. Preparation of the real samples

Recovery studies using real samples were conducted to assess the precision and reliability of the proposed method. These experiments aimed to confirm the applicability of the DSPE–FAAS procedure for extracting Co^{2+} ions from wastewater samples. Real samples were collected directly from the General Directorate of VASKİ (Van Water and Sewerage Administration). Before analysis, the wastewater samples were diluted 50-fold to minimize matrix effects. Spiked samples at defined concentrations were prepared under controlled conditions to simulate realistic wastewater matrices and subsequently analyzed following the optimized extraction procedure.

3. Results and Discussion

The hierarchical three-dimensional (3D) morphology of SbO_2 and $MnSb_2O_6$ particles was examined using high-resolution transmission electron microscopy (HRTEM) and field emission scanning electron microscopy (FESEM). The HRTEM images of $MnSb_2O_6$ revealed a continuous amorphous thin layer, which can be attributed to surface Sb–OH groups. Dispersed nanosized features were observed on the $MnSb_2O_6$ sheets as dark spherical spots (Figure 1a). The interplanar d-spacing of the $MnSb_2O_6$ sheet was determined to be 1.14 nm, corresponding to the [40-40] zone (Figure 1b).

The 3D morphologies of SbO_2 and $MnSb_2O_6$ are shown in Figures 1c and 1d. The undoped SbO_2 particles exhibited flower-like structures composed of cubic sheets, whereas the incorporation of Mn induced a transition to a petal-like morphology in $MnSb_2O_6$. During the solvothermal process, the high NaOH concentration (pH 9–10) promoted a dissolution–recrystallization mechanism, leading to the growth of MnSb(OH) nuclei into petal-shaped architectures (Hu et al., 2007; Liao et al., 2017).

Elemental mapping analysis of the $MnSb_2O_6$ particles confirmed the homogeneous distribution of Mn, Sb, and O within the structure (Figures 1e–g), verifying the successful combination of manganese and antimony oxides in the synthesized material.

The schematic representations of SbO_2 and $MnSb_2O_6$ particles are shown in Figure 2a. SbO_2 crystallizes in the orthorhombic $Pna2_1$ space group, where each Sb atom is coordinated by six oxygen atoms. In contrast, $MnSb_2O_6$ crystallizes in the monoclinic C2/m space group, in which MnO_6 octahedra are interconnected with SbO_6 octahedra to form the overall structure.

The crystal structures of the synthesized particles were verified by X-ray diffraction (XRD) analysis. For SbO_2, prominent diffraction peaks were observed at 2θ = 25.9°, 29.6°, 33.5°, 37.2°, 44.3°, 46.1°, 47.1°, 50.9°, 55.8°, 59.7°, and 60.9°, which were assigned to the (111), (112), (113), (220), (123), (006), (213), (025), (132), (310), and (126) planes, respectively (Figure 2b). These reflections are in

good agreement with the JCPDS card no. 11-0694 (Han et al., 2021). For $MnSb_2O_6$, characteristic diffraction peaks appeared at 2θ = 23.4°, 26.1°, 28.8°, 33.1°, 35.9°, 42.7°, and 55.2°, corresponding to the (110), (111), (200), (220), (310), (400), and (422) planes, respectively. These reflections are consistent with the monoclinic C2/m symmetry and are in close agreement with previously reported $MnSb_2O_6$ reference data (Nalbandyan et al., 2015; Tao et al., 2025). The presence of sharp and well-defined peaks confirms the high crystallinity of the synthesized $MnSb_2O_6$ particles.

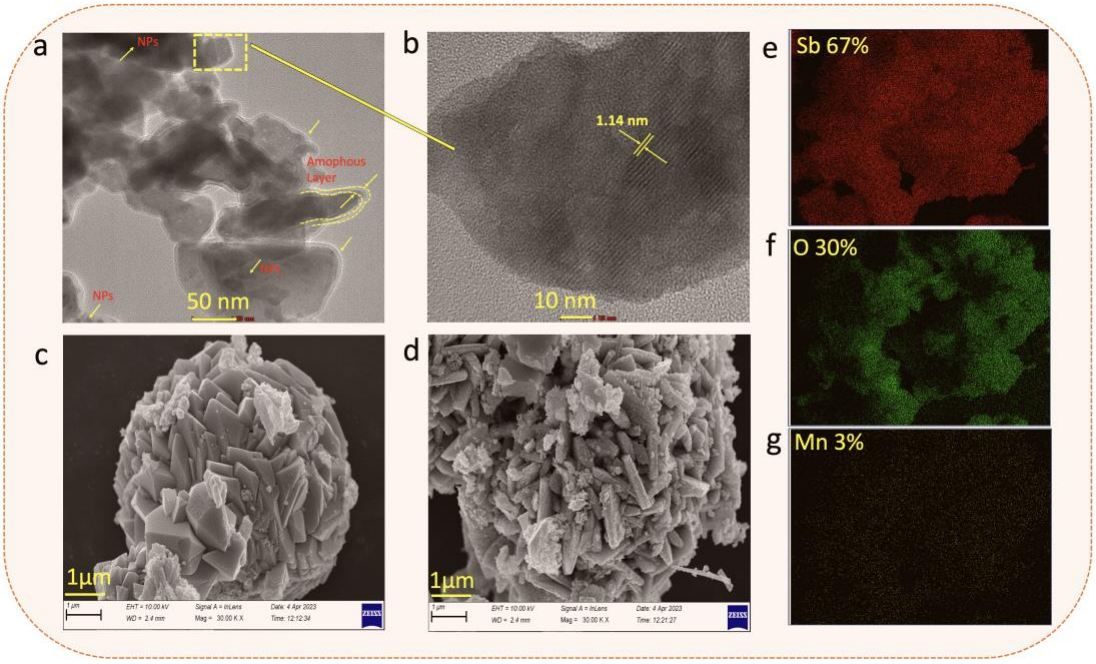

Figure 1. Hierarchical 3D morphology of SbO_2 and $MnSb_2O_6$ particles: (a, b) HRTEM images of $MnSb_2O_6$, (c, d) FESEM images of SbO_2 and $MnSb_2O_6$, and (e–g) elemental mapping of Mn, Sb, and O in $MnSb_2O_6$.

3.1. The electron state and surface chemistry of $MnSb_2O_6$ particles

The survey and high-resolution X-ray photoelectron spectroscopy (XPS) analyses were performed to investigate the binding states, electronic structure, and surface chemistry of the synthesized particles. Figure 2c presents the survey scan, where signals of Sb, Mn, O, and minor C were clearly observed, confirming the successful synthesis of $MnSb_2O_6$ particles and the absence of significant surface contaminants.

The high-resolution XPS spectrum of SbO_2 (Figure 2d) exhibited two distinct Sb 3d peaks at 541.1 eV and 531.7 eV, corresponding to Sb $3d_{3/2}$ and Sb $3d_{5/2}$, respectively. The observed spin–orbit splitting (Δ = 9.4 ± 0.1 eV) is in good agreement with reported values (Gu et al., 2021). While the Sb $3d_{5/2}$ peak partially overlaps with O 1s, the Sb $3d_{3/2}$ peak remains clearly separated. The O 1s region revealed two peaks at 532.0 eV and 530.8 eV, which are attributed to lattice oxygen and surface hydroxyl groups, confirming the presence of surface –OH functionalities that may contribute to adsorption processes (Wagner et al., 1979).

Although the Mn signals were weak in the survey scan, deconvoluted high-resolution spectra (Figure 2c, inset) allowed identification of Mn contributions. Peaks at 641.0 eV, 642.0 eV, 644.8 eV, and 653.0 eV can be assigned to Mn $2p_{3/2}$, Mn^{3+} (Mn_2O_3), Mn^{4+} (MnO_2), and Mn $2p_{1/2}$, respectively. This mixed-valence state of manganese (Mn^{3+}/Mn^{4+}) is consistent with previous reports for Mn-based oxides and provides additional active sites for adsorption through redox and electrostatic interactions (Biesinger et al., 2011). These features confirm the coexistence of Mn and Sb oxidation states on the particle surface.

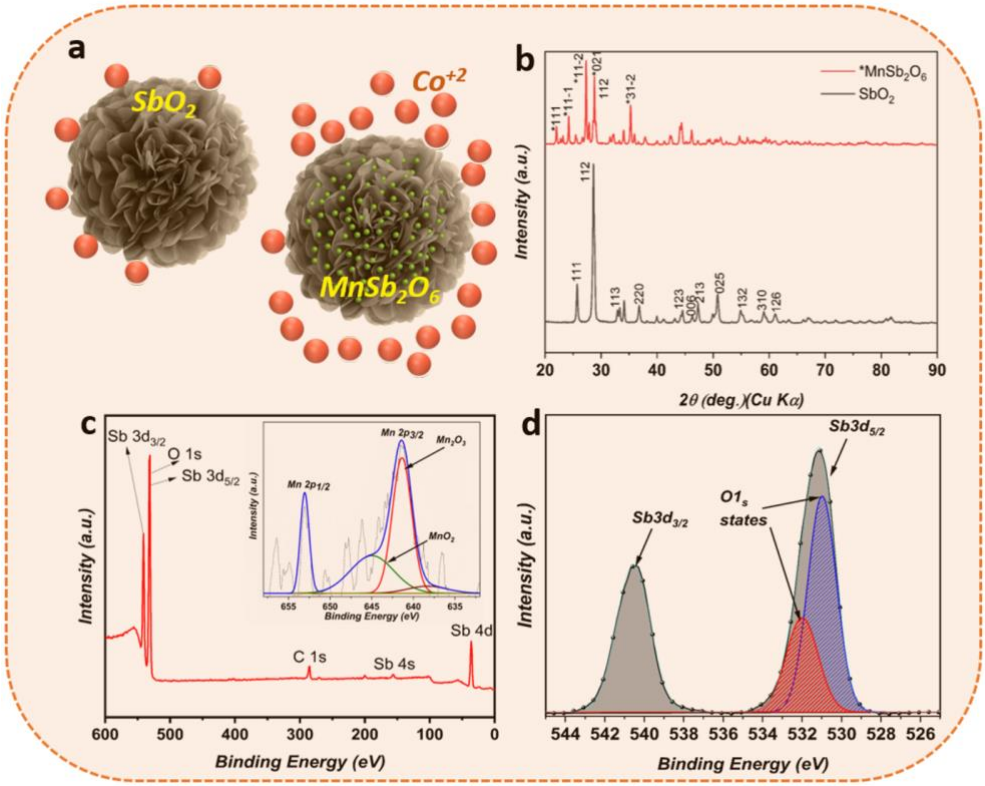

Figure 2. (a) Schematic crystal structures of SbO_2 (orthorhombic $Pna2_1$) and $MnSb_2O_6$ (monoclinic C2/m). (b) XRD patterns of SbO_2 and $MnSb_2O_6$ particles confirming their crystalline phases (c) XPS survey spectrum of $MnSb_2O_6$ with Mn 2p inset showing mixed valence states. (d) High-resolution XPS of Sb 3d and O 1s regions with deconvoluted peaks.

3.2. Analytical method optimization

The MFSP–DSPE–FAAS method was optimized using a univariate approach to improve the signal-to-noise ratio and achieve lower detection limits. This approach systematically evaluates one variable at a time, ensuring reproducibility and high analytical performance. Careful optimization of each critical parameter led to improved precision and accuracy. The optimum values are summarized in Table 1.

3.2.1. Simultaneous optimization of pH and particle types

In heavy metal analysis, solution pH plays a critical role because it influences both the speciation of the analyte and the surface charge of the sorbent. At low pH values, metal ions remain primarily in their free ionic state, but proton competition can suppress adsorption. At higher pH values, metal ions may hydrolyze or precipitate as hydroxides (Unceta et al., 2010). Additionally, the adsorbent surface charge is strongly pH-dependent and influences the electrostatic interaction between metal ions and the sorbent's active sites (Yan et al., 2016). The compatibility between the sorbent surface and hydrated metal species is also controlled by pH (Zhang et al., 2018).

To examine these effects, the performance of magnetic (MFSP) and non-magnetic flower-shaped particles (n-MFSP) was systematically investigated across the pH range 2–13 (Figure 3). This design allowed a simultaneous comparison of sorbent type and solution pH. The results clearly demonstrated that Co^{2+} uptake was strongly dependent on both parameters, with MFSP showing superior enrichment compared to n-MFSP under alkaline conditions.

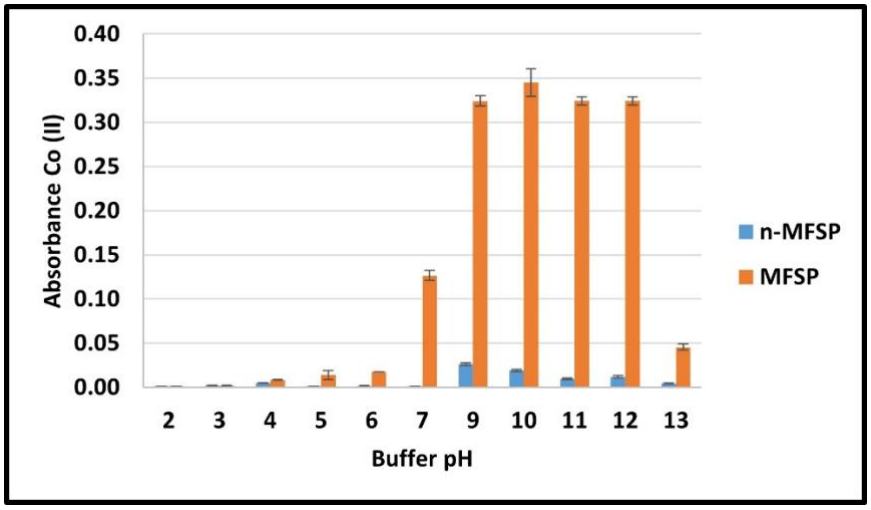

Figure 3. Comparison of average absorbance values of Co^{2+} after DSPE using SbO_2 (n-MFSP) and $MnSb_2O_6$ (MFSP) at different buffer pH levels. Experimental conditions: 0.05 µg mL^{-1} Co^{2+} standard solution (45 mL), 15 mg flower-shaped particles, extraction performed with 1.0 mL pH 10.0 buffer, and desorption with 600 µL HNO_3.

The outcomes of pH optimization for Co^{2+} are presented in Figure 3, demonstrating that the enrichment coefficient of MFSP was superior to that of n-MFSP. A 50 ng mL^{-1} Co^{2+} standard solution was used to calculate the extraction enrichment coefficient. This coefficient was determined by dividing the absorbance value obtained after DSPE treatment by the absorbance value of the same solution measured directly. The enrichment coefficient was 40.75 when MFSP was used and 3.07 with n-MFSP, indicating that the interaction between species with magnetic properties is stronger (Figure 3). Thus, MFSP was identified as the optimal sorbent type for Co^{2+} at pH 10.0. After evaluating different buffer pH levels, pH 10.0 yielded the highest absorbance with acceptable repeatability.

The influence of pH on the adsorption process is noteworthy. At low pH values, the reduced signal is likely due to electrostatic repulsion between the positively charged adsorbent surface, Co^{2+} ions, and the surrounding hydronium ions (Huang et al., 2019). As the pH increases, adsorption becomes more favorable due to enhanced electrostatic attraction between the negatively charged sorbent surface and Co^{2+} ions. Consistently, zeta potential measurements (n = 3) obtained by electrophoretic light scattering revealed that the surface charge of MFSP suspensions shifted monotonically toward more negative values in the pH 7–10 range: –1.0 mV (pH 7), –12.0 mV (pH 8), –18.6 mV (pH 9), and –25.8 mV (pH 10). This trend can be attributed to the progressive deprotonation of ≡M–OH surface groups at increasing pH, leading to the predominance of ≡M–O^- species, and it supports the high preconcentration efficiency observed at pH 10 through electrostatic attraction.

To confirm that precipitation did not interfere with adsorption at pH 10.0, we conducted a control experiment under identical conditions using a blank standard solution. After applying the extraction procedure, the solution was passed through a 0.22 µm membrane filter and analyzed by FAAS. No significant loss of Co^{2+} was detected, confirming that precipitation of $Co(OH)_2$ did not occur under the experimental conditions. Instead, adsorption onto MFSP dominated the removal mechanism. Also, at our trace level (50 ng mL^{-1}; ≈0.85 µM) and pH 10, the ion product $Q = [Co^{2+}][OH^-]^2$ is comparable to literature K_{sp} values for $Co(OH)_2$ (Ksp ≈ 1.6×10^{-15} at 25 °C), but hydrolysis equilibria ($CoOH^+$/$Co(OH)_2$(aq)) reduce free $[Co^{2+}]$; together with the 60 s contact time, this helps explain why bulk hydroxide precipitation was not detected in our filtration control, and adsorption onto MFSP remained the dominant pathway under our conditions (Skoog et al., 1996).

The analyte concentration also significantly influenced the adsorption process. At higher concentrations, removal efficiency increased, while at lower concentrations, adsorption efficiency decreased. This trend reflects the combined effects of electrostatic interactions and magnetic enhancement (Ren et al., 2021). The magnetic property promoted increased mass transfer, improving collision probability between analyte and sorbent and thereby enhancing adsorption selectivity. This

magnetic contribution helps discriminate against competing ions and molecules in the matrix, preventing their diffusion into the sorbent pores (Ren et al., 2021).

Additionally, buffer volume optimization was performed over the range 0.50–2.5 mL. No significant differences were observed in buffering capacity across this range; therefore, 1.5 mL of pH 10 buffer was selected as the optimum volume to ensure high buffering capacity and reproducible extraction efficiency.

3.2.2. Effect of sorbent dosage

Optimizing the sorbent dosage is a critical parameter in the DSPE process, as it directly affects the efficiency of analyte preconcentration. A sufficient surface area must be provided to ensure effective adsorption, while minimizing the eluent volume is necessary for efficient desorption.

To determine the optimal amount, both SbO_2 (n-MFSP) and $MnSb_2O_6$ (MFSP) particles were tested in a 45 mL sample solution over the range 15–50 mg. The absorbance obtained with 40 mg MFSP was approximately 1.3 times higher than that observed with 20 mg and slightly higher than that obtained with 50 mg (Figure 4a). Therefore, 40 mg MFSP was selected as the optimum sorbent dosage for subsequent experiments, providing the best balance between adsorption efficiency and practical applicability.

3.2.3. Optimizing the type and duration of mixing

The optimization of mixing type and duration is crucial for the efficiency of the DSPE process. Proper mixing ensures a homogeneous distribution of analyte and adsorbent and determines the time required to reach adsorption equilibrium, both of which are essential for achieving high sensitivity. Efficient interaction between dissolved metal ions and the active sorbent surface enhances the preconcentration factor.

To investigate this effect, different mixing methods—including magnetic stirring, vortex mixing, mechanical stirring, and manual shaking—were tested. In experiments using 0.25 µg mL^{-1} Co^{2+} solution (45 mL, pH 10.0 buffer) with MFSP as the adsorbent and 600 µL HNO_3 as the eluent, manual shaking produced the highest signal, with an absorbance value 1.4 times greater than that obtained using vortex mixing (Figure 4).

Following identification of the optimal mixing type, the effect of mixing duration was studied at 0, 15, 30, 45, 60, and 90 s. Although prolonged mixing (90 s) resulted in increased variability (%RSD), the absorbance value at 60 s was consistently the highest and reproducible. Therefore, manual shaking for 60 s was selected as the optimal mixing condition for subsequent experiments

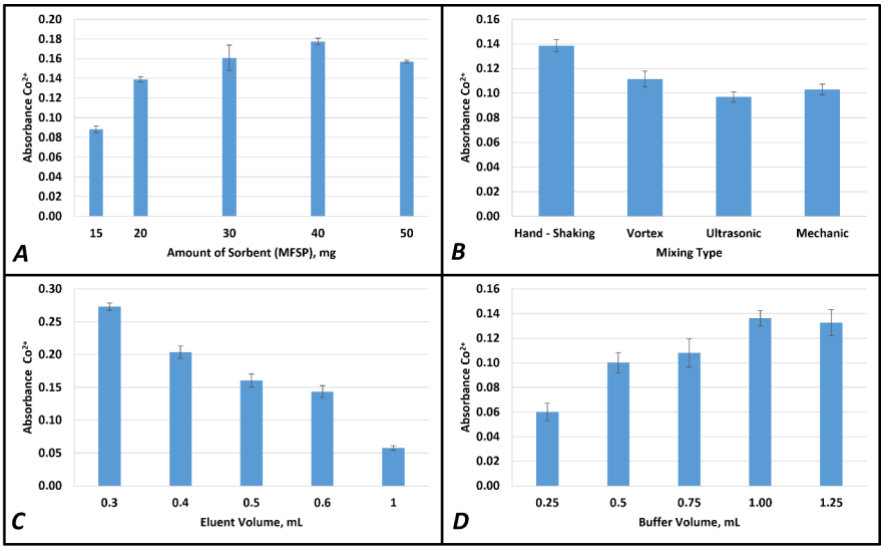

Figure 4. Effect of operational parameters on Co^{2+} preconcentration using MFSP–DSPE–FAAS: (A) sorbent dosage (15–50 mg MFSP), (B) mixing type (manual shaking, vortex, ultrasonic, and

mechanical stirring), (C) eluent volume (0.3–1.0 mL HNO_3), and (D) buffer volume (0.25–1.25 mL at pH 10.0). Experimental conditions: 0.05 μg mL^{-1} Co^{2+} standard solution, 45 mL sample volume, and 300 μL HNO_3 as eluent. Error bars represent standard deviations (n = 3).

3.2.4. The effects of eluent type and volume

Regardless of the efficiency of the adsorption step, an ineffective elution step will ultimately reduce the overall performance of the analytical method. The ideal eluent should completely desorb the analyte from the sorbent, while also enabling easy phase separation without causing centrifugation difficulties.

To identify the most effective eluent, three acids—nitric acid (HNO_3), hydrochloric acid (HCl), and acetic acid—were tested. Acetic acid resulted in the lowest absorbance values, most likely due to the presence of organic residues that can interfere with the flame path in FAAS. Among the tested eluents, HNO_3 provided 1.6-fold higher absorbance than HCl and was therefore selected as the optimal eluent for further experiments.

Subsequently, the effect of eluent volume was examined using 0.3, 0.4, 0.5, 0.6, and 1.0 mL HNO_3 solutions (n = 3 for each condition). As shown in Figure 4c, increasing the eluent volume gradually reduced the enrichment factor due to dilution effects. The best performance was achieved with 0.3 mL HNO_3, which was selected as the optimum volume for subsequent analyses.

3.3. Analytical figures of merit

This study evaluated the performance of flower-shaped particles as DSPE sorbents for Co^{2+} determination by FAAS. The optimized experimental parameters are summarized in Table 1. Under these conditions, the MFSP–DSPE–FAAS method exhibited a dynamic linear range of 5.0–100 ng mL^{-1} for Co^{2+} ions with an excellent correlation coefficient (R^2 = 0.9996). The limit of detection (LOD) and limit of quantification (LOQ) were calculated as 0.295 ng mL^{-1} and 0.984 ng mL^{-1}, respectively. Compared to direct FAAS, the optimized method achieved an 86-fold enhancement in sensitivity.

Table 1. Optimum values of the MFSP-DSPE-FAAS method

Parameter	Optimum Value
Ions	Co^{2+}
Prepared particles	$MnSb_2O_6$
Buffer solution (pH, volume)	pH 10, 1.5 mL
Sorbent dosage	40 mg
Mixing type & duration	Manual shaking, 60 s
Eluent type & volume	HNO_3, 300 μL
FAAS sample flow rate	7.3 mL min^{-1}
Acetylene flow rate	1.0 L min^{-1}

The analytical performance of the proposed method was compared with similar DSPE–FAAS approaches reported in the literature, as shown in Table 2. The MFSP–DSPE–FAAS method achieved LOD and LOQ values that are competitive with or superior to many previously reported sorbent systems, demonstrating its robustness and applicability for trace Co^{2+} determination in environmental samples.

Table 2. MFSP/n-MFSP-DSPE-FAAS method performance and literature comparison

Method and (Analyte)	LOD[a]/LOQ[b] ng mL^{-1}	Linear range ng mL^{-1}	%RSD	EDS[c]	Real Sample	Reference
FAAS/Co^{2+}	24.9/83.1	200-20 000	1.2	-	-	This Study

Table 2. MFSP/n-MFSP-DSPE-FAAS method performance and literature comparison (continued)

MFSP[d]-DSPE-FAAS (Co^{2+})	0.29/0.98	5.0-100	4.7	86	Wastewater	This Study
Fe_3O_4-NPs[f]/MIS-FAAS (Co^{2+})	1.2/4.0	10-55	1.8	180	Water, soil, tea infusion, and vegetable	(Sadıqov et al., 2022)
$Ni(OH)_2$-FSPs[g] /FAAS (Co^{2+})	1.33/4.4	3.0-40	8.15	107.5	Tap water	(Şaylan et al., 2023)
UFP/MNPs/FAAS (Co^{2+})	0.2/-	0.8-150	3.8	50	Water	(Sohrabi-Gilani et al., 2022)
Magnetic TiO2-mPs@S based SPE (Co^{2+})	0.23	-	0.41	20	Tap water, lake water, and wastewater	(Diriba et al., 2025)

[a] Limit of detection, [b] Limit of quantification, [c] Enrichment in detection sensitivity, [d] $MnSb_2O_6$, [e] SbO_2, [f] Fe_3O_4 nanoparticles, [g] $Ni(OH)_2$ nanoflowers.

3.4. Application of the method to real samples

To evaluate the applicability of the developed method to complex environmental samples, recovery studies were performed using a domestic wastewater sample collected from the General Directorate of VASKİ–Van Water and Sewerage Administration (Table 3). Wastewater contains numerous potential interferents, including detergents, soaps, oils, greases, pesticides, and organic residues from household activities (Mara, 2013). To minimize matrix effects, the sample was diluted 1:50 and treated as a blank matrix for Co^{2+} determination.

When the MFSP–DSPE–FAAS method was directly applied to the diluted blank sample, no measurable signal was obtained, confirming the absence of detectable Co^{2+}. Therefore, a matrix-matched calibration strategy was employed. The wastewater samples were spiked with Co^{2+} at concentrations of 20, 50, and 75 ng mL^{-1}, and recovery values were calculated under the optimized experimental conditions.

As shown in Table 3, the recoveries ranged from 94.3% to 107.5%, with acceptable precision (RSD < 8%). These results fall well within the reported acceptable range for recovery in trace analysis 60–115%, (González & Herrador, 2007), demonstrating that the MFSP–DSPE–FAAS method is accurate and reliable for Co^{2+} determination in complex wastewater matrices.

Table 3. Recovery results for Co^{2+} in wastewater samples (n = 3)

	Wastewater		
Initial Concentration	**Co^{2+} Spiked Concentration** *ng mL^{-1}*	**Found Concentration** *ng mL^{-1}*	**Recovery % ± SD**
<LOD (not detected)	20	18.9	94.3 ± 6.2
	50	53.8	107.5 ± 7.1
	75	74.5	99.3 ± 5.2

3.5. Effect of interfering ions

In this study, the selectivity of the developed MFSP–DSPE–FAAS method against common coexisting ions was evaluated to confirm its robustness in realistic wastewater matrices. Transition

metals (1.0 mg L^{-1}; Ni^{2+}, Cr^{3+}, Cd^{2+}, Fe^{3+}, Zn^{2+}) and macro-ions (40 mg L^{-1}; Mg^{2+}, Ca^{2+}/Cl^-, K^+/NO_3^-, Na^+/Cl^-, SO_4^{2-}) were spiked into solutions containing 50 ng mL^{-1} Co^{2+}. The observed recoveries ranged from 78–90% for transition metals and 81–90% for macro-ions (Table 4). These results indicate that ions with similar hydration radii and Lewis acidity (e.g., Ni^{2+}, Cd^{2+}, Zn^{2+}) can partially compete with Co^{2+} for active adsorption sites, while monovalent salts (Na^+, K^+, Cl^-, NO_3^-) primarily influence ionic strength, leading to limited suppression. Comparable trends have been reported for DSPE/MSPE sorbents in trace metal preconcentration, where transition metals exhibit competitive adsorption while bulk electrolytes remain largely tolerable (Korkmaz et al., 2025; Sürme et al., 2024).

Table 4. Effect of coexisting ions on the recovery of 50 ng mL^{-1} Co^{2+} using the MFSP–DSPE–FAAS method (n = 3)

Ion	Added salt	Concentration (mg L^{-1})	Recovery (%)
Ni^{2+}	$Ni(NO_3)_2$	1.0	80.2 ± 9.8
Cr^{3+}	$Cr(NO_3)_3$	1.0	81.3 ± 6.2
Cd^{2+}	$CdCl_2 \cdot H_2O$	1.0	79.3 ± 9.4
Fe^{3+}	$Fe(NO_3)_3$	1.0	85.4 ± 8.1
Zn^{2+}	$Zn(NO_3)_2$	1.0	78.3 ± 8.9
Mg^{2+}	$MgCl_2$	40	89.2 ± 7.8
Cl^-, Ca^{2+}	$CaCl_2$	40	81.0 ± 9.1
NO_3^-, K^+	KNO_3	40	89.7 ± 5.3
Na^+, Cl^-	NaCl	40	90.1 ± 6.2
SO_4^{2-}	Na_2SO_4	40	80.4 ± 6.1

4. Conclusion

In conclusion, this study demonstrated the effectiveness of hierarchical $MnSb_2O_6$ flower-shaped particles (MFSP) as dispersive solid-phase extraction (DSPE) adsorbents for the determination of Co^{2+} ions by flame atomic absorption spectrometry (FAAS). The optimized method exhibited a dynamic linear range of 5.0–100 ng mL^{-1}, with excellent correlation (R^2 = 0.9996), and provided low detection and quantification limits (LOD: 0.295 ng mL^{-1}, LOQ: 0.984 ng mL^{-1}). Compared to direct FAAS, the MFSP–DSPE–FAAS method achieved an 86-fold enhancement in sensitivity.

The applicability of the method was validated through recovery studies on wastewater samples obtained from the General Directorate of VASKİ–Van Water and Sewerage Administration. Despite the complexity of the matrix, the method yielded recoveries in the range of 94–108%, confirming its robustness and reliability for real environmental samples. The use of matrix-matched calibration effectively minimized interferences and further ensured accuracy.

A key finding of this work is the demonstration of the role of magnetic properties in enhancing adsorption selectivity and efficiency. The comparison between magnetic ($MnSb_2O_6$) and non-magnetic (SbO_2) flower-shaped particles clearly showed that magnetic interactions significantly promoted Co^{2+} uptake. This highlights the specificity of MFSP as sorbents and underscores their potential for broader applications in environmental monitoring and trace heavy metal determination.

Acknowledgements

This study was supported by Van Yüzüncü Yıl University Scientific Research Projects Coordination Unit under the project number FHD-2024-11276. The authors gratefully acknowledge the support provided by the Van Yüzüncü Yıl University Science Research and Application Centre (https://www.yyu.edu.tr/images/files/Lab_Catalogue_Final.pdf) for material characterization analyses.

Conflict of Interest Statement

The author confirms that no known financial or personal conflicts of interest could have influenced the work reported in this manuscript.

Research and Publication Ethics Statement

The author declares that the research and publication ethics were fully observed throughout the study.

Ethics Committee Approval Statement

The author declares that the materials and methods used in this study did not require ethics committee approval and/or any special legal permission.

Data Availability Statement

The author declares that the data generated and analyzed during this study are available from the author upon reasonable request. No external data repository was used for this work.

Artificial Intelligence Use Statement

The author declares that generative artificial intelligence tools were used only for language editing and text refinement during the preparation of this manuscript. No AI tools were used for generating data, figures, tables, analyses, or scientific content. The author takes full responsibility for the integrity and accuracy of the final manuscript.

References

Ahmadi, M., Elmongy, H., Madrakian, T., & Abdel-Rehim, M. (2017). Nanomaterials as sorbents for sample preparation in bioanalysis: A review. *Analytica Chimica Acta*, *958*, 1-21. https://doi.org/10.1016/j.aca.2016.11.062

Alav, A., Kutlu, N., Kına, E., & Meral, R. (2024). A novel green tea extract-loaded nanofiber coating for kiwi fruit: Improved microbial stability and nutritional quality. *Food Bioscience*, *62*, 105043. https://doi.org/10.1016/j.fbio.2024.105043

Ali, H., Khan, E., & Ilahi, I. (2019). Environmental chemistry and ecotoxicology of hazardous heavy metals: environmental persistence, toxicity, and bioaccumulation. *Journal of chemistry*, *2019*. https://doi.org/10.1155/2019/6730305

Ali, O. I., & Azzam, A. B. (2023). Functional Ag-EDTA-modified MnO2 nanocoral reef for rapid removal of hazardous copper from wastewater. *Environmental Science and Pollution Research*, *30*(59), 123751-123769. https://doi.org/10.1007/s11356-023-30805-0

Azzouz, A., Kailasa, S. K., Lee, S. S., Rascón, A. J., Ballesteros, E., Zhang, M., & Kim, K.-H. (2018). Review of nanomaterials as sorbents in solid-phase extraction for environmental samples. *TrAC Trends in Analytical Chemistry*, *108*, 347-369. https://doi.org/10.1016/j.trac.2018.08.009

Baskin, D. (2025a). Preconcentration and Determination of Copper (II) in Water and Tea Infusion Samples Using Hierarchical MnSb2O6@ Fe3O4 Nanoparticles and Magnetic Solid Phase Extraction–FAAS. *ACS Omega*, *10*(9), 9537-9546. https://doi.org/10.1021/acsomega.4c10772

Baskin, D. (2025b). Spinel ZnFe2O4 Nanoparticles Doped with Ba2+ for High-Performance Cu (II) Extraction via d-SPE–FAAS. *ACS Omega*. https://doi.org/10.1021/acsomega.5c07865

Baskın, D., Yılmaz, Ö., Islam, M. N., Tülü, M., Koyuncu, İ., & Eren, T. (2021). Metal adsorption properties of multi-functional PAMAM dendrimer based gels. *Journal of Polymer Science*, *59*(14), 1540-1555. https://doi.org/10.1002/pol.20210210

Bhargava, P., Gupta, N., Vats, S., & Goel, R. (2017). Health issues and heavy metals. *Austin J Environ Toxicol*, *3*(1), 3018.

Biesinger, M. C., Payne, B. P., Grosvenor, A. P., Lau, L. W., Gerson, A. R., & Smart, R. S. C. (2011). Resolving surface chemical states in XPS analysis of first row transition metals, oxides and

hydroxides: Cr, Mn, Fe, Co and Ni. *Applied Surface Science*, *257*(7), 2717-2730. https://doi.org/10.1016/j.apsusc.2010.10.051

Büyüktiryaki, S., Keçili, R., & Hussain, C. M. (2020a). Functionalized nanomaterials in dispersive solid phase extraction: Advances & prospects. *TrAC Trends in Analytical Chemistry*, *127*, 115893. https://doi.org/10.1016/j.trac.2020.115893

Büyüktiryaki, S., Keçili, R., & Hussain, C. M. (2020b). Modern age of analytical chemistry: nanomaterials. In *Handbook of nanomaterials in analytical chemistry* (pp. 29-40). Elsevier. https://doi.org/10.1016/B978-0-12-816699-4.00002-5

Cimboláková, I., Uher, I., Laktičová, K. V., Vargová, M., Kimáková, T., & Papajová, I. (2020). Heavy metals and the environment. *Environ. Factors Affect. Hum. Heal*, *10*. https://doi.org/10.5772/intechopen.86876

da Costa, M. A. J. L., Costa, M. F., Sorrentino, R., Carvalho, N. M., & de Gois, J. S. (2024). A new approach for the determination of As, Cu, and Pb in seawater samples using manganese oxide octahedral molecular sieve as a sorbent for dispersive solid-phase microextraction. *Talanta*, *268*, 125320. https://doi.org/10.1016/j.talanta.2023.125320

Diriba, F., Amde, M., & Teju, E. (2025). Sulfide-modified magnetic titanium dioxide microparticles for the adsorption and solid-phase extraction of toxic metals in aqueous samples. *Journal of Dispersion Science and Technology*, *46*(5), 699-712. https://doi.org/10.1080/01932691.2023.2298872

González, A. G., & Herrador, M. Á. (2007). A practical guide to analytical method validation, including measurement uncertainty and accuracy profiles. *TrAC Trends in Analytical Chemistry*, *26*(3), 227-238. https://doi.org/10.1016/j.trac.2007.01.009

Gu, T., Teng, W., Liu, A., Deng, Z., Ling, L., & Zhang, W.-x. (2021). Transformation of nanoscale zero-valent iron with antimony: Effects of the Sb spatial configuration. *Chemical Engineering Journal*, *416*, 129073. https://doi.org/10.1016/j.cej.2021.129073

Hagarová, I., & Nemček, L. (2021). Application of metallic nanoparticles and their hybrids as innovative sorbents for separation and pre-concentration of trace elements by dispersive micro-solid phase extraction: A minireview. *Frontiers in Chemistry*, *9*, 672755. https://doi.org/10.3389/fchem.2021.672755

Haghighi, S. M. N., & Kazemi, N. M. (2021). Separation and determination of lithium and manganese ions in healthy humans and multiple sclerosis patients based on Nano graphene oxide by Ultrasound assisted-dispersive-micro solid-phase extraction. *Analytical Methods in Environmental Chemistry Journal*, *4*(04), 20-35. https://doi.org/10.24200/amecj.v4.i04.158

Han, Z., Zheng, J., Kong, F., Tao, S., & Qian, B. (2021). One dimensional SbO2/Sb2O3@ NC microrod as anode for lithium-ion and sodium-ion batteries. *Nano Select*, *2*(2), 425-432. https://doi.org/10.1002/nano.202000092

Hu, Y., Zhang, H., & Yang, H. (2007). Direct synthesis of Sb2O3 nanoparticles via hydrolysis-precipitation method. *Journal of alloys and compounds*, *428*(1-2), 327-331. https://doi.org/10.1016/j.jallcom.2006.03.057

Huang, D., Wu, J., Wang, L., Liu, X., Meng, J., Tang, X.,…& Xu, J. (2019). Novel insight into adsorption and co-adsorption of heavy metal ions and an organic pollutant by magnetic graphene nanomaterials in water. *Chemical Engineering Journal*, *358*, 1399-1409. https://doi.org/10.1016/j.cej.2018.10.138

İnce, M. N., Serbest, H., & Bakirdere, S. (2024). Microwave-assisted synthesis of antimony oxide nanoparticles for the determination of trace cadmium in mulberry leaf tea matrices by flame atomic absorption spectrophotometry. *Journal of Analytical Science and Technology*, *15*(1), 55. https://doi.org/10.1186/s40543-024-00469-7

Keçili, R., & Hussain, C. M. (2018). Recent progress of imprinted nanomaterials in analytical chemistry. *International journal of analytical chemistry*, *2018*. https://doi.org/10.1155/2018/8503853

Korkmaz, Ş., Hasanoğlu Özkan, E., Uzun, D., Kurnaz Yetim, N., & Özcan, C. (2025). Magnetic Solid Phase Extraction of Lead (II) and Cadmium (II) From Water Samples Using ZnO@Fe3O4 Nanoparticles Combined With Flame Atomic Absorption Spectrometry Determination. *Journal of Separation Science*, *48*(3), e70115. https://doi.org/10.1002/jssc.70115

Li, Q., He, Y., Yang, A., Hu, X., Liu, F., Mu, J.,…& Yang, L.-P. (2023). Antimony (III) removal by biogenic manganese oxides formed by Pseudomonas aeruginosa PA-1: kinetics and

mechanisms. *Environmental Science and Pollution Research*, *30*(43), 97102-97114. https://doi.org/10.1007/s11356-023-29277-z

Liao, Y., He, L., Zhao, M., & Ye, D. (2017). Ultrasonic-assisted hydrothermal synthesis of ceria nanorods and their catalytic properties for toluene oxidation. *Journal of environmental chemical engineering*, *5*(5), 5054-5060. https://doi.org/10.1016/j.jece.2017.09.037

Lin, S., Pan, X., Meng, D., & Zhang, T. (2021). Electric conversion treatment of cobalt-containing wastewater. *Water Science and Technology*, *83*(8), 1973-1986. https://doi.org/10.2166/wst.2021.101

Mafakheri, N., Shamsipur, M., & Babajani, N. (2024). Development of a dispersive liquid–liquid microextraction procedure based on a natural deep eutectic solvent for ligand-less preconcentration and determination of heavy metals from water and food samples. *Microchemical Journal*, *199*, 110010. https://doi.org/10.1016/j.microc.2024.110010

Mara, D. (2013). *Domestic wastewater treatment in developing countries*. Routledge. https://doi.org/10.4324/9781849771023

Nalbandyan, V. B., Zvereva, E. A., Nikulin, A. Y., Shukaev, I. L., Whangbo, M.-H., Koo, H.-J.,…& Vasiliev, A. N. (2015). New phase of MnSb2O6 prepared by ion exchange: Structural, magnetic, and thermodynamic properties. *Inorganic Chemistry*, *54*(4), 1705-1711. https://doi.org/10.1021/ic502666c

Oviedo, M. N., Luján, C. E., Lemos, A. A., Botella, M. B., Llaver, M., & Wuilloud, R. G. (2024). An overview of preconcentration techniques combined with inductively coupled plasma mass spectrometry for trace element determination in biological studies. *Analytical and Bioanalytical Chemistry*, *416*(11), 2641-2656. https://doi.org/10.1007/s00216-024-05124-z

Öner, M., Demir, C., Çetin, G., & Bakırdere, S. (2023). Development of a rapid and efficient analytical method for trace lead determination: Manganese dioxide nanoflower based dispersive solid-phase extraction. *Measurement*, *211*, 112606. https://doi.org/10.1016/j.measurement.2023.112606

Qi, W., Guo, S., Sun, H., Liu, Q., Hu, H., Liu, P.,… & Zhang, M. (2022). Synthesis and characterization of Sb2O3 nanoparticles by liquid phase method under acidic condition. *Journal of Crystal Growth*, *588*, 126642. https://doi.org/10.1016/j.jcrysgro.2022.126642

Rehman, K., Fatima, F., Waheed, I., & Akash, M. S. H. (2018). Prevalence of exposure of heavy metals and their impact on health consequences. *Journal of cellular biochemistry*, *119*(1), 157-184. https://doi.org/10.1002/jcb.26234

Ren, J., Zhu, Z., Qiu, Y., Yu, F., Ma, J., & Zhao, J. (2021). Magnetic field assisted adsorption of pollutants from an aqueous solution: A review. *Journal of Hazardous Materials*, *408*, 124846. https://doi.org/10.1016/j.jhazmat.2020.124846

Sadıqov, E., Elyas Sodan, N., Siyal, A. N., Elçi, A., & Elçi, L. (2022). Determination of cobalt and copper in water, plant, and soil samples by magnetite nanoparticle-based solid-phase microextraction (SPME) coupled with microsample injection system-flame atomic absorption spectrometry (MIS-FAAS). *Instrumentation Science & Technology*, *50*(4), 351-369. https://doi.org/10.1080/10739149.2021.2002891

Salamat, Q., & Soylak, M. (2024). Magnetic covalent organic frameworks-based adsorbents in solid phase extraction of trace analytes in environmental samples. *Trends in Environmental Analytical Chemistry*, *41*, e00222. https://doi.org/10.1016/j.teac.2023.e00222

Skoog, D. A., West, D. M., Holler, F. J., & Crouch, S. R. (1996). *Fundamentals of analytical chemistry* (Vol. 33). Saunders College Pub. Fort Worth.

Sohrabi-Gilani, N., Ghayournezhad, A., & Rostamzadeh Mansour, S. (2022). Determination of ultratrace levels of cobalt (II) and chromium (III) by magnetic dispersive solid-phase extraction (SPE) using urea-formaldehyde polymer/magnetite nanoparticles with flame atomic absorption spectrometry (FAAS). *Analytical Letters*, *55*(16), 2650-2667. https://doi.org/10.1080/00032719.2022.2067863

Sürme, Y., Kahve Yıldırım, G., Uçan, M., & Narin, İ. (2024). Ultrasound-enhanced dispersive solid phase extraction of Cd (II), Co (II), and Ni (II) using magnetic Pinus pinea. *Microchemical Journal*, *196*, 109648. https://doi.org/https://doi.org/10.1016/j.microc.2023.109648

Şaylan, M., Demirel, R., Ayyıldız, M. F., Chormey, D. S., Çetin, G., & Bakırdere, S. (2023). Nickel hydroxide nanoflower–based dispersive solid-phase extraction of copper from water matrix.

Environmental Monitoring and Assessment, *195*(1), 133. https://doi.org/10.1007/s10661-022-10653-0

Tao, J., Xiong, P., Wang, R., Ma, Q., Li, B., Li, H.,…& Zhang, C. (2025). A facile synthesis of MnSb2O6 anode material with enhanced Li-storage performance. *Journal of Alloys and Compounds*, *1014*, 178797. https://doi.org/10.1016/j.jallcom.2025.178797

Tong, Y., Liu, X., & Zhang, L. (2019). One-pot fabrication of magnetic porous Fe 3 C/MnO/graphitic carbon microspheres for dispersive solid-phase extraction of herbicides prior to their quantification by HPLC. *Microchimica Acta*, *186*, 1-9. https://doi.org/10.1007/s00604-019-3358-0

Unceta, N., Séby, F., Malherbe, J., & Donard, O. F. X. (2010). Chromium speciation in solid matrices and regulation: a review. *Analytical and Bioanalytical Chemistry*, *397*, 1097-1111. https://doi.org/10.1007/s00216-009-3417-1

Wagner, C., Riggs, W., Davis, L., Moulder, J., & Muilenberg, G. (1979). Handbook of X-ray photoelectron spectroscopy, Perkin-Elmer Corp. *Eden Prairie, MN*, *38*.

Wehmeier, S., Preihs, M., Dressler, J., Raab, A., & Feldmann, J. (2024). Detection of inorganic arsenic in rice using a field-deployable method with Cola extraction. *Analytical and Bioanalytical Chemistry*, *416*(11), 2677-2682. https://doi.org/10.1007/s00216-023-05041-7

Yan, H., Yang, H., Li, A., & Cheng, R. (2016). pH-tunable surface charge of chitosan/graphene oxide composite adsorbent for efficient removal of multiple pollutants from water. *Chemical Engineering Journal*, *284*, 1397-1405. https://doi.org/10.1016/j.cej.2015.06.030

Zhang, L., Cao, W., Alvarez, P. J., Qu, X., Fu, H., Zheng, S.,…& Zhu, D. (2018). Oxidized template-synthesized mesoporous carbon with pH-dependent adsorption activity: A promising adsorbent for removal of hydrophilic ionic liquid. *Applied Surface Science*, *440*, 821-829. https://doi.org/10.1016/j.apsusc.2018.01.211